

EXECUTION-ERROR MODELING AND ANALYSIS OF THE GRAIL SPACECRAFT PAIR

Troy D. Goodson*

The GRAIL spacecraft, Ebb and Flow (aka GRAIL-A and GRAIL-B), completed their prime mission in June and extended mission in December 2012. The excellent performance of the propulsion and attitude control subsystems contributed significantly to the mission's success. In order to better understand this performance, the Navigation Team has analyzed and refined the execution-error models for ΔV maneuvers. There were enough maneuvers in the prime mission to form the basis of a model update that was used in the extended mission. This paper documents the evolution of the execution-error models along with the analysis and software used.

INTRODUCTION

The Gravity Recovery and Interior Laboratory (GRAIL) mission operated two spacecraft in flight from September 2011 through December 2012, spanning the prime and extended missions. The spacecraft, Ebb (GRAIL-A) and Flow (GRAIL-B), executed seventy-eight (78) ΔV maneuvers in total. Of these, fifty-seven (57) were main-engine maneuvers that could be used to refine the execution-error model. The remainder were either executed with the Attitude Control Subsystem (ACS) thrusters, involved rotation of the spacecraft during the burn, operated at a low duty-cycle, or did not cut-off based on the accelerometer.

The two spacecraft were not precisely identical. However, the elements of their propulsion system, notably the locations of the ACS thrusters and main-engine were identical and are shown in Figure 1. The figure omits thrusters ACS-5 and ACS-6, which were placed opposing ACS-7 and ACS-8. Where ACS-7's location may be described as (-Y,-Z) and ACS-8's as (+Y,-Z), then ACS-5 was located (+Y,+Z) and ACS-6 was (-Y,+Z) using the Y and Z spacecraft axes noted in the figure.

Thrust from the main-engine produced a ΔV in the +X direction. That ΔV was oriented inertially by slewing the spacecraft with reaction wheels, once from the reference attitude to the burn attitude and another reversed the process. Executed on reaction wheels, these slews did not produce additional ΔV .

The prime mission required a large number of maneuvers, mostly due to the needs of the Orbit Period Reduction (OPR) phase. In the extended mission, a large number of Eccentricity Correction Maneuvers (ECMs) were necessary because the orbit was not stable, due to the non-uniform nature of the gravity field at the Moon. The gravity field caused the eccentricity and argument of periapsis to change with time such that the altitude of the ascending node of the orbit decreased and the altitude of the descending node increased. The altitude of the science orbit for the extended mission

*Engineering Staff, Section 343, Jet Propulsion Laboratory, California Institute of Technology, Mail Stop 264-282, 4800 Oak Grove Dr, Pasadena, CA 91109

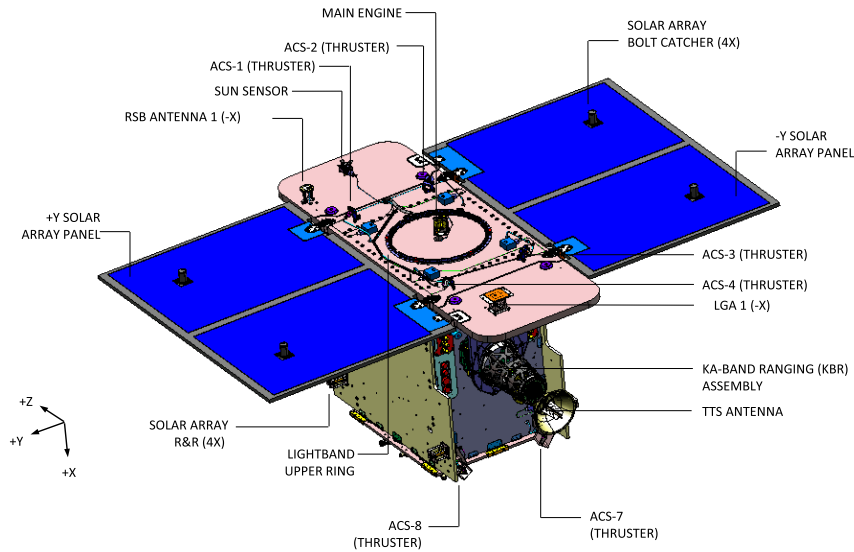


Figure 1. GRAIL S/C Configuration. ACS-5 was located (+Y,+Z) and ACS-6 was located (-Y,+Z), opposite to ACS-7 and ACS-8

was chosen to be as low as possible such that the orbit lifetime was approximately two weeks. Each week, a pair of ECMs reset this condition.¹

Midway into the prime mission, it became clear that the maneuver $\Delta\vec{V}$ pointing errors weren't matching the pre-launch model and the magnitude errors might be better than the model. Out of 25 main-engine maneuvers at that point, four (4) should've been larger than 1.8σ for pointing errors; GRAIL had seven (7). For magnitude errors, there should've been about seven (7) above 1σ ; GRAIL had only two (2).

The prime mission had been designed to be robust in the presence of larger execution errors; the extended mission was less tolerant. The navigation team performed a statistical analysis of the maneuvers in the prime mission to better judge mission performance and assist in planning the extended mission.

MODEL FOR EXECUTION ERRORS

Maneuver execution errors for GRAIL are in the form of the Gates model. The Gates model² accounts for magnitude and pointing errors due to six independent error sources, each Normally distributed. Magnitude errors are defined as errors that are parallel to the commanded or nominal $\Delta\vec{V}$ direction. These errors are the sum of two independent sources, fixed and proportional magnitude errors. Fixed magnitude errors are assumed to be Normally distributed, $N(0, \sigma_1^2)$. Proportional magnitude errors are assumed to have a standard deviation proportional to ΔV magnitude, giving $N(0, (\sigma_2\Delta V)^2)$.

Pointing errors are perpendicular to the nominal $\Delta\vec{V}$ direction and assumed to be identically distributed in any direction of that plane, referred to as the pointing plane. They are modeled as the vector sum of contributors along two perpendicular axes, \vec{X} and \vec{Y} , spanning the pointing plane. Along either axes, the errors are the sum of fixed and proportional pointing errors as $N(0, \sigma_3^2)$ and $N(0, (\sigma_4\Delta V)^2)$. This pointing model is referred to as a per-axis model.

The total pointing model is an alternative to the per-axis pointing model. In the total pointing model, pointing errors are assumed to have directions, in the pointing plane, that measure as angle θ from \vec{X} with a uniform distribution across 360° . The length of the pointing error, Δv_p , is a random variable of a Rayleigh distribution with parameter $\sigma_p = \sqrt{\sigma_3^2 + (\sigma_4 \Delta V)^2}$. The standard deviation of the length of the pointing error is

$$\sigma_{\Delta v_p} = \sigma_p \sqrt{\frac{4 - \pi}{2}} = \sqrt{\frac{4 - \pi}{2}} (\sigma_3^2 + (\sigma_4 \Delta V)^2) \quad (1)$$

These two alternative pointing models are equivalent^{3,4} but note that the standard deviation of the length of the total pointing error is not equal to the standard deviation of the per-axis pointing error.

In a coordinate system whose first axis is parallel to the commanded $\Delta \vec{V}$, the Gates model gives the following covariance matrix for the execution-error vector:

$$P = \begin{pmatrix} \sigma_m^2 & 0 & 0 \\ 0 & \sigma_p^2 & 0 \\ 0 & 0 & \sigma_p^2 \end{pmatrix} = \begin{pmatrix} \sigma_1^2 + v^2 \sigma_2^2 & 0 & 0 \\ 0 & \sigma_3^2 + (\sigma_4 \Delta V)^2 & 0 \\ 0 & 0 & \sigma_3^2 + (\sigma_4 \Delta V)^2 \end{pmatrix} \quad (2)$$

where ΔV is the magnitude of the maneuver $\Delta \vec{V}$, σ_1 and σ_2 are the fixed and proportional Gates-model parameters for magnitude, and σ_3 and σ_4 are the fixed and proportional Gates-model parameters for pointing. The symbol σ_m is the overall standard deviation of magnitude errors and σ_p is likewise for pointing errors, per axis. For any particular $\Delta \vec{V}$, the Gates model describes a multivariate Normal distribution $N(0, P)$.

Different values were assigned to the model parameters for different classes of maneuvers. This was partly due to the variety of ways the GRAIL mission executed maneuvers and partly due to the expected gradual improvement in calibrations.

MANEUVER DESCRIPTIONS

The GRAIL prime mission was divided into seven phases: Launch, Trans-Lunar Cruise (TLC), Lunar Orbit Insertion (LOI), OPR, Transition to Science Formation (TSF), Science (SCI), and Decommissioning. These phases are depicted in Fig. 2, drawn along Earth's orbit around the Sun. More detail on each mission phase may be found in Ref.5 which also has more details on trajectory design.

The extended mission (XM) also included several phases, starting with the Lunar Eclipse (LEC) phase (which replaced the Decommissioning phase of the original mission), then the Low Beta-Angle (LBA) phase, the Transition to Science Formation XM (TSF-XM), the Science XM (SCI-XM) phase, and finally a new Decommissioning phase. All of these are shown in Fig. 3, arranged similarly to Figure 2.

The main-engine maneuvers of TLC were used to ensure accurate delivery to the Lunar sphere of influence. These maneuvers were referred to as Trajectory Correction Maneuvers (TCMs). After the project decided to cancel TCM-A1 and TCM-B1, the first maneuvers available to calibrate maneuver execution were TCM-A2 and TCM-B2. Furthermore, the project canceled TCM-A5 and TCM-B5. During TLC, an error was discovered and corrected in a transformation matrix for the inertial measurement unit (IMU).⁶ The last maneuvers before reaching lunar orbit were TCM-A4 and TCM-B4, both of which were relatively small and executed with the main engine operating at 15% duty cycle. Furthermore, TCM-A4 cut-off with the maximum-burn timer instead of the

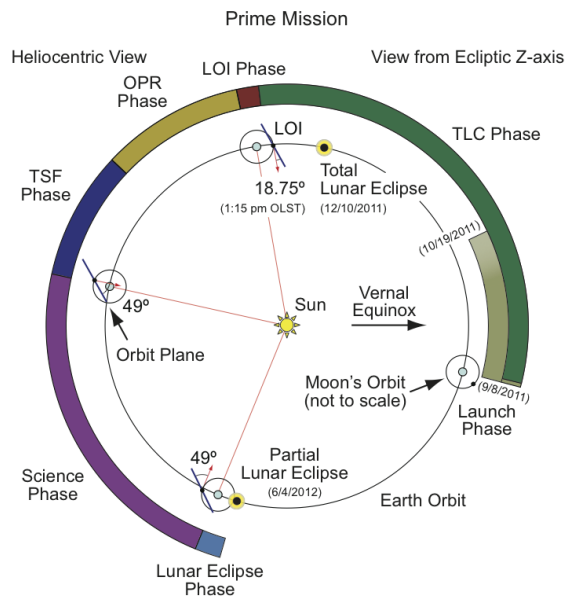


Figure 2. Phases of the Prime Mission

intended accelerometer.^{6,7} Consequently, TCM-A4 and TCM-B4 are excluded from the execution-error analysis.

Strictly speaking, the spacecraft arrived at the Moon into an elliptical orbit. However, the orbit was quite large and required some reduction to ensure that perturbing accelerations would not eject the spacecraft from the lunar sphere of influence. On 31 December 2011 and 1 January 2012, respectively, the LOI-A and LOI-B maneuvers reduced the orbit period to about 11.4 hours. Both LOIs were pitch-over maneuvers, they were performed while the spacecraft was rotating, and so were also excluded from the execution-error analysis.

LOI was followed by OPR with the first Period Reduction Maneuver (PRM) on 14 January 2012. Maneuvers PRM-A1 through PRM-A7 and PRM-B1 through PRM-B7, were executed near lunar periaapses and reduced the orbit period to a little less than two (2) hours. All fourteen (14) of these maneuvers were executed with the main-engine and cut off with the accelerometer. None of them were excluded from the analysis.

During this phase and, in particular with the PRMs, the navigation team took notice that these maneuvers were large enough so that uncertainty in burn duration became an important contributor to achieving the target orbital period. These were maneuvers where it would have been useful to consider thrust uncertainty as an element of the execution-error model. The maneuvers cut-off on ΔV and, assuming no other errors, thrust errors became duration errors which affected the location of the centroid of the maneuver. In this way, the correct $\Delta \vec{V}$ might not achieve the desired change in period because of the effective location of the maneuver.

The ACS team noted that the onboard controller's performance had been limited on some maneuvers due to apparent shifts in the location of the spacecraft's center of mass. Maneuvers PRM-B3, PRM-B4, and PRM-B5 were notable for apparent shifts of the center of mass.

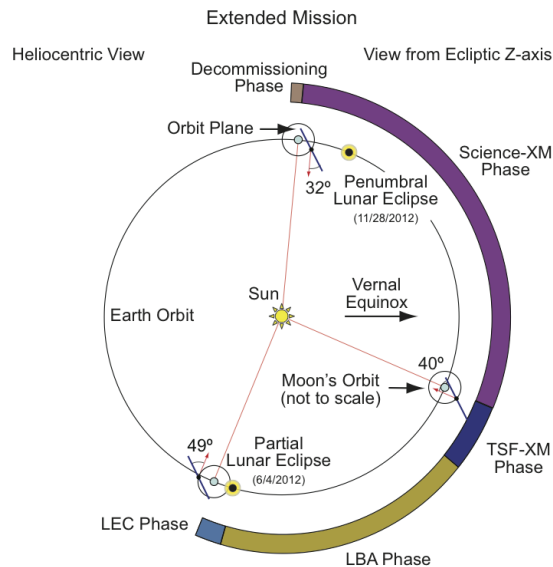


Figure 3. Phases of the Extended Mission

The maneuvers of the TSF phase were Transition to Science Maneuvers (TSMs) and Orbit Trim Maneuvers (OTMs). The OTMs were executed with the ACS thrusters resulting in their exclusion from the execution-error analysis. These maneuvers brought the two spacecraft into a leader-follower formation with GRAIL-B in the lead position. The TSMs used the main engine and an inertially-fixed spacecraft attitude, so they were included in this analysis. The ACS team reported a shift in center of mass between PRM-A7 and TSM-A1, and then during TSM-B2.

A lunar eclipse punctuated the time period between the primary and extended missions, referred to as the LEC phase. At the beginning of this phase, both spacecraft's orbits had short lifetimes, consistent with the now-defunct decommissioning phase of the prime mission. The first maneuvers of the extended mission, the Orbit Circularization Maneuvers (OCMs), one for each spacecraft, raised this orbit to extend lifetime, increased the distance between spacecraft for safety, and avoided the need for further maneuvers until well after the lunar eclipse. The OCMs were each about 16 m/s and circularized the orbit to approximately 84 km altitude. Furthermore, by performing OCM-B1 first, the formation was reversed so that GRAIL-A moved into the lead position. The reversal was necessary because the extended mission's science phase occurred on the other side of the Sun. The ACS team noted a shift of center of mass during OCM-B1.

The maneuver OTM-B3 was the sole correction during the next phase, the LBA phase. It retargeted the separation distance to 665 km to prepare for the TSF-XM phase. OTM-B3 was executed with the ACS thrusters and not included in the execution-error analysis.

The TSF-XM phase was not as complicated as the TSF phase of the prime mission and included maneuvers ECM-A1, ECM-B1, OTM-A1, ECM-A2, ECM-B2, and OTM-A2. These maneuvers established the orbit geometry for the start of the SCI-XM phase. The ECMs were main-engine maneuvers and the OTMs used ACS thrusters; the former were included and the latter excluded. A shift in the center of mass seemed to have occurred either before or at the beginning of ECM-B1, according to ACS. ECM-B2 also saw a shift.

In the SCI-XM phase, the ECM and OTM pattern continued every week up to ECM-A16, ECM-B16, and OTM-A16. These maneuvers maintained approximately two weeks of orbit lifetime at an altitude of approximately 23 km above the reference sphere. In the third week, however, the maneuvers weren't necessary and were skipped. The ACS team reported shifts in the center of mass for ECM-B4, ECM-B6, ECM-B7, ECM-B9, ECM-B10, and ECM-B11.

The SCI-XM phase was followed by a decommissioning phase. Lunar impact was targeted with ECM-A17 and ECM-B17. Both spacecraft's fuel tanks were depleted with maneuvers BTD-A and BTD-B as an engineering experiment. As these BTD maneuvers cut-off on an acceleration threshold (0.058 m/s^2) via the accelerometer, instead of ΔV they were not included in the execution-error analysis. Impact occurred on 17 December 2012.

The ACS team routinely updated parameters of the attitude controller in an active effort to reduce maneuver execution-errors. The feed-forward torque settings were updated on the following maneuvers: PRMs A1 and B1; TSMs A1, B2, and B3; ECMs A1, B1, A4, A5, B5, B7, A9, A10, A11, A12, A13, A14, B14, A15, A16, A17, and B17. The main-engine alignment vector was updated for PRMs A1, B1, and B2; TSMs A1, B1, A2 and B3; ECMs A2, A9, A14, and B15.

PRE-LAUNCH EXECUTION-ERROR MODEL DESCRIPTION

As described earlier, the execution-error models used by GRAIL were in the form of the Gates model. The parameters of the model varied according to maneuver. These parameters were initially set before launch in the so-called Pre-Launch Model⁸ as listed in Table 1. In that table, TCM-1 refers to both TCM-A1 and TCM-B1 and likewise for other maneuver names. The TCM-1 maneuvers have their own model to account for being the first maneuvers and, as such, not calibrated. The parameters for TCM-2 maneuvers reflect the initial calibration and so on for the TCM-3 through TSM-B1 maneuvers. The parameters for TCM-4 and TCM-5 maneuvers reflect assumptions for 15% duty cycling of the main engine as these maneuvers were expected to be relatively small. The parameters for TSM-B2 and TSM-B3 reflect an assumption of further improvements in ACS calibration. Finally, the table includes parameters for the OTMs, which were all ACS-thruster maneuvers.

MAXIMUM-LIKELIHOOD ESTIMATION

The updates to the Gates-model parameters in this analysis were determined with maximum-likelihood estimation (MLE).⁹ This is interpreted as maximizing the likelihood that the resulting model parameters could've generated the observed execution errors. A similar process has been used for data from Cassini-Huygens.¹⁰

If every engine firing was for the same commanded $\Delta \vec{V}$, then the samples would be of the same Normal distribution. One could compute the sample standard deviation of magnitude error samples to use as an estimate of σ_m . Unfortunately, it would not be possible to solve directly from this result for the contributions of the fixed and proportional terms, σ_1 and σ_2 .

When, as is the case here, each maneuver has a different commanded $\Delta \vec{V}$, each sample is from a different Normal distribution. It is also notable that the covariance matrices of these distributions are nonlinearly related, so that there isn't a linear transformation that would reveal an underlying common covariance matrix. The Gates model provides a relationship for these different distributions that may be exploited for the maximum-likelihood method.

Table 1. Pre-Launch Execution-Error Model (3- σ).

	Magnitude		Pointing	
	Fixed (m/s)	Proportional (%)	Fixed (m/s)	Proportional (mrad)
TCM-1	0.007	0.25	0.003	<ul style="list-style-type: none"> • 50 mrad for $\Delta V < 5$ m/s • linear decrease from 50 mrad at 5 m/s to 10 mrad at 20 m/s • 10 mrad for $\Delta V > 20$ m/s
TCM-2	0.007	0.25	0.001	10
TCM-3 - TSM-B1	0.007	0.25	0.001	5
TCM-4, TCM-5	0.00105	1.667	0.001	6
TSM-B2, TSM-B3	0.007	0.25	0.001	4
OTMs	0.00003	6.00	0.0003	120

(Proportional pointing values are for total pointing at 99.7 percentile, fixed pointing values are per axis.)

First, the probability density function (pdf) for the magnitude error is

$$f_m(x, v, \mu_1, \mu_2, \sigma_1, \sigma_2) = [2\pi(\sigma_1^2 + v^2\sigma_2^2)]^{-1/2} \exp\left[-\frac{1}{2} \frac{(x - \mu_1 - v\mu_2)^2}{\sigma_1^2 + v^2\sigma_2^2}\right] \quad (3)$$

where x is the magnitude error, v is the ΔV magnitude, μ_1 is the fixed error bias, and μ_2 is the proportional error bias. Then, the likelihood function for magnitude errors, L_m , is defined as the product of evaluations of f_m for each measurement:

$$L_m(\mu_1, \mu_2, \sigma_1, \sigma_2) = \prod_{i=1}^N f_m(x_i, v_i, \mu_1, \mu_2, \sigma_1, \sigma_2) \quad (4)$$

For the pointing error vector, the pdf is

$$f_p(\vec{x}, v, \vec{\mu}_3, \vec{\mu}_4, \sigma_3, \sigma_4) = [\sqrt{2\pi}(\sigma_3^2 + v^2\sigma_4^2)]^{-1} \exp\left[-\frac{1}{2} \frac{|\vec{x} - \vec{\mu}_3 - v\vec{\mu}_4|^2}{\sigma_3^2 + v^2\sigma_4^2}\right] \quad (5)$$

where \vec{x} is the pointing error vector in units of velocity, $\vec{\mu}_3$ is the fixed pointing error bias, and $\vec{\mu}_4$ is the proportional pointing error bias. The likelihood function for pointing errors, L_p , is then defined as follows:

$$L_p(\vec{\mu}_3, \vec{\mu}_4, \sigma_3, \sigma_4) = \prod_{i=1}^N f_p(\vec{x}_i, v_i, \vec{\mu}_3, \vec{\mu}_4, \sigma_3, \sigma_4) \quad (6)$$

A weighted maximum-likelihood approach is to raise each term in the likelihood function to a power. For the magnitude errors, the exponent is the inverse of the reconstruction's 1- σ uncertainty. For pointing errors, the uncertainty is two-dimensional, so the inverse of the standard deviation of the error along the pointing-error direction is used.

The Gates-model parameters for magnitude and pointing errors are found by maximizing L_m and L_p , respectively. Maximizing such a large product leads to some problems; a common approach is to maximize the logarithm of L_m or L_p , which, instead, involves a summation of terms and an equivalent maximization.⁹ The bias terms μ_1 , μ_2 , $\vec{\mu}_3$, and $\vec{\mu}_4$ may be either considered free parameters in the maximization problem or fixed constants chosen by some other method.

Update Based on the Prime Mission

At the end of the prime mission, execution-error results were collected and a maximum-likelihood estimation of the model parameters was performed. In doing so, all appropriate main-engine maneuver execution errors were assumed to originate with one set of model parameters. This idea also extended to the assumption that both spacecraft had identical propulsion systems so that GRAIL-A and GRAIL-B data could be combined. All the maneuvers described earlier as included in the analysis were grouped together.

The prelaunch model of Table 1 gave a-priori estimates of the model parameters. As the mission progressed, our knowledge of the system improved. The prelaunch model attempted to account for that incremental improvement. The maximum likelihood estimation produced a-posteriori estimates; a reconstruction of the model parameters.

Table 2 lists execution-error data for all maneuvers of the prime mission. The epoch listed is the start of the maneuver in UTC. The column $\Delta\vec{V}$ is the commanded maneuver magnitude. Under “Magnitude”, μ_{OD} is the Orbit Determination (OD) estimated magnitude error computed as estimate minus commanded. Next, σ_{OD} is the standard deviation of the uncertainty in the OD estimate. Third, Δ_{ACS} is the magnitude estimate from ACS minus the OD estimate. Under pointing, Y_{OD} and Z_{OD} are the estimated pointing errors, estimate minus design, in the spacecraft coordinate system as denoted in Figure 1. The column “OD 1- σ Ellipse” gives the semimajor and semiminor axes of the OD 1- σ uncertainty as projected into the spacecraft’s Y,Z plane. The angle is degrees counter-clockwise from the Y axis. Then “ ΔY_{ACS} ” and “ ΔZ_{ACS} ” are the ACS estimate minus the OD estimate. Finally, the three columns “Mag,” “Ptg,” and “Tot” give the OD error estimate divided by the standard deviation for magnitude, pointing, and the root-sum-square of both. Note that these are one-, two-, and three-dimensional distributions, respectively.

In the prime mission, GRAIL-A and GRAIL-B had executed 14 and 17 trajectory-correction maneuvers, respectively, for a total of 31. Of these, 12 and 13, respectively, were included in the analysis. Details of these execution errors are listed in Table 2. Statistical testing of these 25 main-engine maneuvers against the pre-launch model showed statistical issues for both pointing and magnitude error models. Too many maneuvers had large pointing errors. Specifically, pointing errors should follow a two-dimensional Normal distribution, in which 4 out of 25 (16.4%) are larger than 1.8σ . GRAIL had *seven* (7) (almost double) as listed below:

- PRM-A1 (1.9σ), PRM-A2 (2.6σ), PRM-A3 (2.2σ), TSM-A1 (5.5σ)
- TCM-B2 (1.8σ), PRM-B5 (1.9σ), TSM-B2 (5.1σ)

Too few maneuvers had large magnitude errors. These should’ve followed a one-dimensional Normal distribution, in which 7 out of 25 (31.7%) are above 1σ . GRAIL had only *two* (2): TSM-B2 (1.6σ), TSM-B3 (2.6σ). Note that the number of σ quoted here reference the pre-launch model, Table 1, and does not match Table 2 because that corresponds to the “August 2012” model, discussed later.

Table 2. Maneuver Execution Errors

Mnvr	Epoch (UTC)	$\Delta \vec{V}$ (m/s)	Magnitude				Pointing				Mag # σ	Ptg #	Tot # σ
			μ_{OD} (mm/s)	σ_{OD} (mm/s)	Δ_{ACS} (mm/s)	Y_{OD} (mrad)	Z_{OD} (mrad)	OD 1- σ Ellipse (μ rad)	ΔY_{ACS} (mrad)	ΔZ_{ACS} (mrad)			
TCM-A2	30-SEP-11 18:00	13.968	0.11	0.45	-1.00	4.3	0.1	38.8 x 6.5, 4.5°	-0.2	0.3	0.01	1.48	1.48
TCM-B2	05-OCT-11 18:00	25.096	-7.23	0.45	-1.48	-1.0	5.2	20.2 x 7.1, -4.1°	2.5	-1.6	0.34	1.83	1.86
TCM-A3	16-NOV-11 18:00	6.454	-2.58	0.53	-1.37	0.4	1.1	154.7 x 10.5, 2.7°	-0.2	0.6	0.82	0.47	0.95
TCM-B3	21-NOV-11 18:00	8.845	-2.68	0.52	0.76	3.8	2.4	101.5 x 10.4, -3.8°	0.1	0.0	0.35	1.54	1.58
TCM-A4	09-DEC-11 18:00	0.234	-5.24	0.36	-0.51	1.5	0.8	1709.5 x 1093.3, 1.6°	0.0	-1.5	3.90	0.75	3.97
TCM-B4	14-DEC-11 18:00	0.257	-0.50	0.35	-0.31	-0.3	-0.7	1329.4 x 765.3, -7.0°	-0.6	0.9	0.34	0.35	0.49
PRM-A1	07-JAN-12 13:36	79.286	-32.30	1.26	25.94	4.2	3.5	95.9 x 36.1, -7.0°	1.7	-1.5	0.49	1.86	1.92
PRM-A2	08-JAN-12 17:21	79.286	-18.13	1.48	13.77	2.6	7.0	571.8 x 72.2, -3.6°	2.4	-6.3	0.27	2.57	2.58
PRM-A3	09-JAN-12 17:30	79.286	-22.06	2.80	20.10	2.6	5.9	374.6 x 12.6, -3.2°	-0.3	-2.8	0.33	2.22	2.24
PRM-B1	13-JAN-12 21:00	74.109	15.56	1.88	-2.36	1.5	1.5	50.4 x 27.9, 2.6°	-1.0	-1.3	1.35	0.86	1.60
PRM-B2	15-JAN-12 01:35	74.109	3.66	2.06	-6.66	1.2	1.2	11.4 x 5.3, 4.3°	-1.5	-0.3	0.32	0.67	0.74
PRM-B3	16-JAN-12 02:50	74.109	-8.69	2.20	4.49	0.1	0.9	14.1 x 2.0, -1.8°	0.7	0.1	0.75	0.38	0.85
PRM-A4	24-JAN-12 15:29	69.544	-8.38	1.25	9.89	2.9	2.6	573.6 x 4.3, 2.5°	-1.0	-1.3	0.14	1.34	1.34
PRM-A5	25-JAN-12 18:20	69.544	-6.87	1.05	2.78	2.6	1.4	781.8 x 27.6, 5.5°	-0.0	1.4	0.12	1.00	1.01
PRM-A6	26-JAN-12 16:58	69.544	-14.00	0.63	13.01	4.3	0.9	130.1 x 16.5, 6.6°	-0.3	1.0	0.24	1.52	1.54
PRM-A7	27-JAN-12 16:48	69.544	-4.90	0.96	1.61	3.0	1.2	52.3 x 9.5, 6.8°	0.3	0.6	0.08	1.13	1.13
PRM-B4	31-JAN-12 16:29	70.634	28.00	0.64	-30.67	0.4	2.0	119.5 x 20.7, -6.6°	0.1	1.5	2.54	0.83	2.67
PRM-B5	01-FEB-12 17:23	70.634	3.98	0.17	-3.54	1.5	2.3	62.4 x 7.9, -5.2°	0.6	-0.4	0.36	1.08	1.14
PRM-B6	02-FEB-12 16:48	70.634	-3.48	1.68	8.11	1.9	0.8	1010.4 x 132.0, -2.2°	-0.0	-0.3	0.32	0.83	0.89
PRM-B7	03-FEB-12 17:20	70.634	0.55	0.06	-0.02	0.6	2.2	12.7 x 3.3, 6.1°	0.0	-0.7	0.05	0.90	0.90
TSM-A1	07-FEB-12 16:32	8.234	-3.92	0.16	-0.85	5.4	-5.9	89.5 x 7.7, 0.8°	0.0	0.8	1.21	3.21	3.43
TSM-B1	14-FEB-12 03:15	17.495	-1.31	0.44	3.41	0.4	1.6	47.7 x 21.6, -2.0°	-0.1	0.0	0.33	0.66	0.74
TSM-A2	20-FEB-12 15:05	19.276	2.25	0.95	-0.80	0.3	-0.9	37.5 x 14.9, 4.0°	-0.3	0.3	0.54	0.39	0.66
TSM-B2	24-FEB-12 17:24	2.065	-4.61	1.43	-1.92	1.1	7.3	1138.1 x 151.6, -3.4°	1.0	0.3	1.53	2.97	3.34
TSM-B3	29-FEB-12 13:46	0.507	-6.07	0.79	-1.52	-0.8	-1.2	1542.0 x 734.4, -0.7°	-0.9	1.7	2.02	0.58	2.10

Estimation of parameters for GRAIL's pointing errors was complicated by changes in ACS configuration throughout the mission. In particular, the ACS team often estimated a new main-engine alignment vector. The burn attitude of the maneuver was then determined so as to align this vector with the desired $\Delta\vec{V}$ direction. The OD estimates, which were expressed in Earth Mean Equator of J2000.0, were converted to pointing errors by transforming coordinates to the spacecraft axes of Fig. 1 and differencing from the main-engine alignment vector. This has the effect of projecting the pointing error in the Y-Z spacecraft axes plane and ignores only a minimal component of the pointing error.

The ACS attitude controller's feedforward gains were adjusted to compensate for movement of the center of mass. This did not appear to cause any particularly troublesome biases in the data and so no attempt was made to adjust the data to compensate for the effect.

The magnitude errors in this data set are plotted in Figure 5. The pointing error magnitudes are plotted in Figure 6. Some more insight into the pointing data is provided by Figure 4, which plots OD's pointing error estimates in the pointing plane spanned by the spacecraft's Y and Z coordinate axes from Figure 1. The ΔV errors were divided by the magnitude of the design ΔV to give angles. Ellipses representing the $1\text{-}\sigma$ OD uncertainty are plotted around each point, in accordance to Table 2. Of particular interest at this point in the mission was that most of the data resides in the first quadrant of the plot and it was not clear if this represented a real bias or was due to insufficient data.

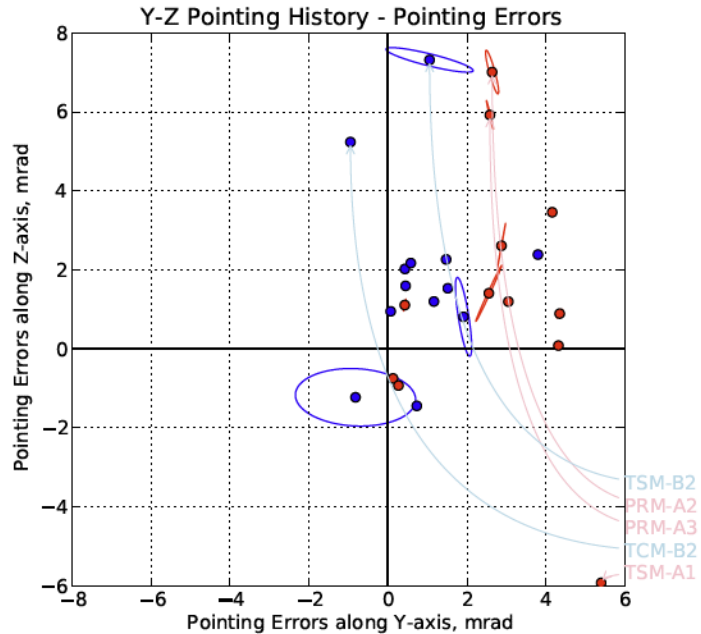


Figure 4. Pointing Errors in the Y-Z Plane for the Prime Mission.

The resulting model is listed in Table 3. Figures 5 and 8 show the model plotted on top of the data sets. In Figure 5, the dark line represents the computed biases and the dashed lines represent 1σ and 3σ of the estimated model. Red data points are from GRAIL-A's maneuvers and blue data

Table 3. Estimate for Prime Mission Main-Engine Maneuvers (1- σ)

	Fixed	Proportional
mag. bias	-1.5195 mm/s	-0.0050 %
mag. std. dev.	2.6213 mm/s	0.0150 %
ptg. bias Y	0.0000 mm/s	0.0000 mrad
ptg. bias Z	0.0000 mm/s	0.0000 mrad
ptg. std. dev.	0.0000 mm/s	2.5018 mrad

points are from GRAIL-B's. Each data point is surrounded by its OD estimate uncertainty, which also is how the samples were weighted. Figure 8 has the same features except the bias parameters are accounted for in the plotted data (though in this case, the biases are zero) and the dark lines represent 1σ and 3σ of the estimated model.

To validate the estimated models, Figures 6 and 9 show how well the number of samples matches the cumulative density function. These are typical probability-probability plots that show, on the vertical scale, how many samples fall into the range of ΔV values corresponding to the probability levels of the cumulative density function noted on the horizontal scale. If the tops of the bars perfectly match a diagonal line, then the samples precisely match the model. The degree to which this condition is achieved is rated on a scale from 0 to 1 by the Chi-squared (χ^2) test.⁹ For the magnitude distribution, the result is 0.99 and for the pointing distribution, the result is 0.86. These were deemed satisfactory. Further support for this fit is seen in Figures 7 and 10. These plots show the number of σ indicated by a samples location in the sorted list of samples versus the number of σ indicated by the sample's value. Again, if the data fall on a straight line, the fit is ideal. The pointing data is clearly not fit as well as the magnitude data, but the result is good enough.

The magnitude errors appeared to have a negligible proportional bias (error in accelerometer scale factor) and a small fixed bias of 2 to 3 mm/s. These bias values were computed by a weighted average instead of the MLE process because it improved the result of a χ^2 fitness test. The pointing errors showed a proportional pointing bias of roughly 2.5 mrad and 3.0 mrad in Y and Z S/C axes, respectively, similar to recent ACS assessments. Fixed pointing biases were not as clear, but results were on the order of 1 mm/s. For the maximum-likelihood estimation, the pointing-error biases were forced to zero and only the standard deviations were estimated.

Based on engineering judgement, the magnitude-error estimated biases were ignored and other values were rounded to produce model parameters named "August 2012 Main Engine" and listed in Table 4. This was the model used in planning the extended mission and, later, to evaluate maneuver performance during the extended mission.

Table 4. "August 2012 Main Engine" Execution-Error Model, Prime Mission Performance (3- σ)

	Fixed	Proportional
Magnitude	9.0 mm/s	0.045 %
Pointing	0.0 mm/s	7.5 mrad

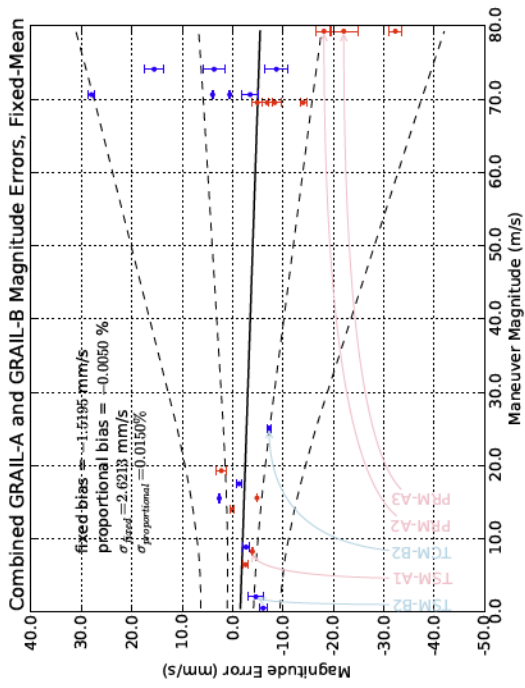


Figure 5. August 2005 Model Mag. Residuals

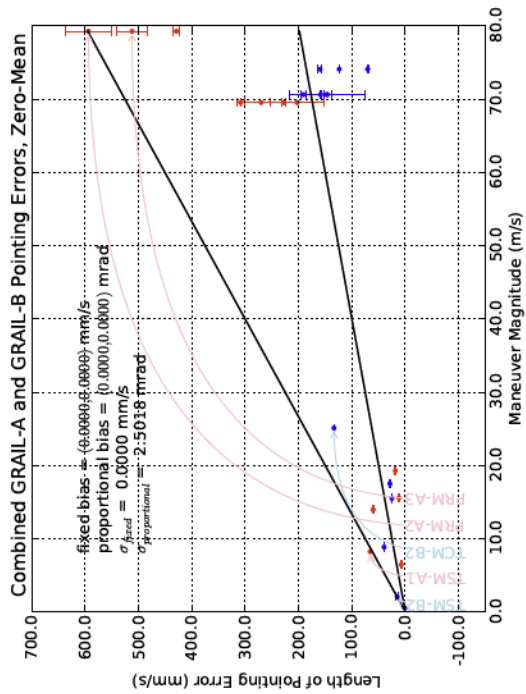


Figure 6. August 2005, Mag. Prob.

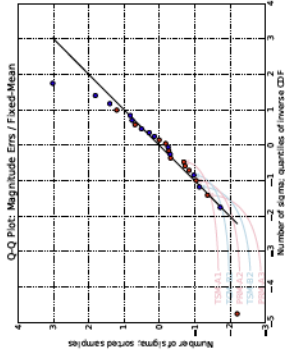


Figure 7. August 2005, Mag. Q-Q

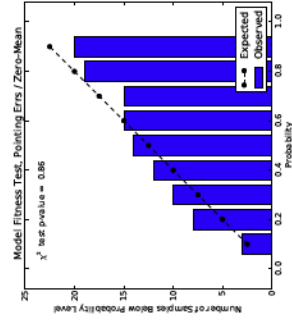


Figure 8. August 2005 Model Mag. Residuals

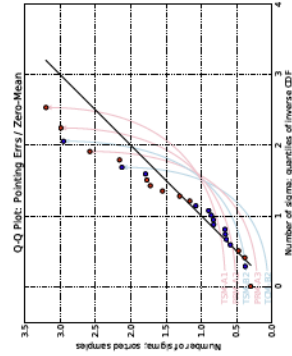


Figure 9. August 2005, Ptg. Prob.

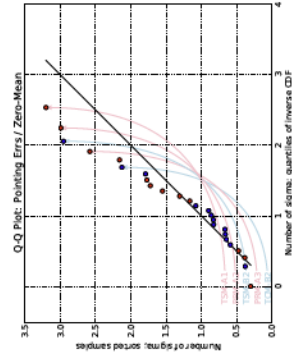


Figure 10. August 2005, Ptg. Q-Q

Update Based on All Maneuvers

Although the Navigation team continued to monitor execution-error performance, no further in-flight update to the execution-error model was recommended. Only after the completion of the mission was a final estimate of the execution-error model settled upon. The maneuver data for the extended mission are listed in Table 5.

Early in the extended mission, it became clear that pointing errors were somewhat smaller than the “August 2012” model. One possible explanation is that during the extended mission, the lower fuel levels limited the motion of the spacecraft’s center of mass. This would have allowed the ACS controller to perform better than in the prime mission.

There were fifty-seven (57) main engine maneuvers that were considered for this estimation. The magnitude errors are plotted in Fig. 12 in the same manner as before, as are the pointing errors plotted in Fig. 15, both with commanded maneuver magnitude on the horizontal axis. The individual components of the pointing in Y and Z spacecraft coordinates are plotted in Figure 11. It is striking in this plot to see the other quadrants filled in. This seems to indicate that what appears to be a bias in Fig. 4 is only a symptom of the lack of data.

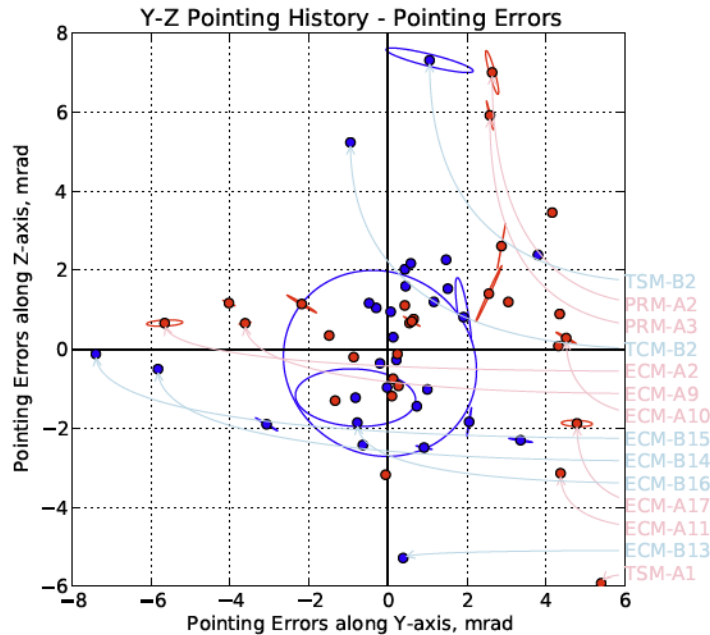


Figure 11. Pointing Errors in the Y-Z Plane for All Maneuvers, Prime and Extended Missions.

Some of these maneuvers in Fig. 11 appear to be outliers. The number of σ as listed in Table 5 don't seem to be excessive, but they lie in the fringe areas of the pointing plane. The maneuvers in question are as follows: ECM-A10 at 1.81σ , ECM-A17 at 2.06σ , ECM-A11 at 2.14σ , ECM-B15 at 2.96σ , ECM-B13 at 2.12σ , PRM-A2 at 2.57σ , and ECM-A2 at 2.27σ . These maneuvers were not included when estimating the model, but they are included in Figures 12-17 and their exclusion seems to improve the fit of the model. The χ^2 fitness test for the pointing model of Table 6 is 0.98

Table 5. Maneuver Execution Errors of the Extended Mission

Mnvr	Epoch (UTC)	$\Delta \vec{V}$ (m/s)	Magnitude			Pointing					Mag # σ	Pg # σ	Tot # σ
			μ_{OD} (mm/s)	σ_{OD} (mm/s)	Δ_{ACS} (mm/s)	Y_{OD} (mrad)	Z_{OD} (mrad)	OD 1- σ Ellipse (μ rad)	ΔY_{ACS} (mrad)	ΔZ_{ACS} (mrad)			
OCM-A1	30-MAY-12 21:34	15.550	-4.84	0.06	-0.30	0.1	-0.7	28.9 x 10.8, 7.0°	-0.2	0.5	1.27	0.30	1.31
OCM-B1	30-MAY-12 19:39	15.511	2.64	0.06	-0.66	0.7	-1.4	27.9 x 13.7, -4.8°	0.3	0.0	0.70	0.65	0.95
ECM-A1	20-AUG-12 17:54	38.341	3.78	1.31	-3.66	0.1	-1.2	21.3 x 7.6, -7.2°	0.4	-0.5	0.58	0.48	0.75
ECM-B1	20-AUG-12 16:04	37.602	18.18	2.59	-20.69	0.2	-0.3	38.9 x 16.9, -6.6°	0.2	-0.2	2.85	0.14	2.85
ECM-A2	27-AUG-12 18:12	10.208	23.62	1.31	-23.15	-5.6	0.7	456.6 x 76.8, 0.7°	6.4	-1.1	7.01	2.27	7.37
ECM-B2	27-AUG-12 16:22	10.537	-4.59	0.04	-0.18	1.0	-1.0	33.4 x 3.6, 6.2°	-0.1	0.1	1.35	0.57	1.47
ECM-A4	10-SEP-12 15:14	10.056	-3.68	0.04	-0.04	0.2	-0.1	27.2 x 7.1, -4.5°	-0.1	0.1	1.10	0.11	1.10
ECM-B4	10-SEP-12 15:15	9.684	-3.95	0.05	0.21	-0.6	-2.4	31.8 x 7.3, 5.1°	0.1	-0.0	1.18	0.10	1.10
ECM-A5	17-SEP-12 16:51	9.909	-4.02	0.28	3.06	0.6	0.8	35.9 x 9.2, 7.1°	-0.4	0.1	1.20	0.40	1.26
ECM-B5	17-SEP-12 16:51	10.059	-6.00	0.30	3.37	-0.3	1.1	32.4 x 8.5, -6.2°	0.3	0.1	1.79	0.44	1.84
ECM-A6	24-SEP-12 11:16	9.779	-6.45	0.06	0.14	0.6	0.7	244.3 x 11.2, -6.3°	-0.6	0.5	1.93	0.37	1.97
ECM-B6	24-SEP-12 11:17	9.781	-4.33	0.09	-0.81	2.1	-1.8	365.2 x 11.7, 2.2°	-0.3	-1.6	1.30	1.10	1.70
ECM-A7	01-OCT-12 14:25	8.028	2.25	0.79	-1.93	0.5	0.7	104.1 x 14.3, 1.8°	-0.2	0.6	0.70	0.34	0.78
ECM-B7	01-OCT-12 14:26	8.048	-2.39	0.74	-2.54	-0.0	-1.0	69.0 x 13.7, 5.1°	0.4	0.4	0.74	0.39	0.83
ECM-A8	08-OCT-12 15:40	5.907	-6.16	0.15	-0.34	-2.2	1.1	436.7 x 24.7, -6.3°	1.4	-0.7	1.97	0.99	2.20
ECM-B8	08-OCT-12 15:41	5.939	1.80	0.12	-1.00	-3.1	-1.9	323.8 x 14.2, -6.3°	-0.3	0.3	0.58	1.45	1.56
ECM-A9	15-OCT-12 15:35	9.482	13.19	1.45	-15.98	-3.6	0.7	158.7 x 25.1, 2.1°	0.7	0.6	3.97	1.47	4.23
ECM-B9	15-OCT-12 15:36	9.457	8.81	1.08	-8.06	-0.5	1.2	79.0 x 19.9, 4.6°	0.1	-0.1	2.66	0.50	2.70
ECM-A10	22-OCT-12 09:54	8.529	-1.38	0.16	-1.22	4.5	0.3	294.2 x 21.2, -6.2°	0.5	-0.1	0.42	1.81	1.86
ECM-B10	22-OCT-12 09:55	8.510	-2.31	0.16	-0.84	3.4	-2.3	308.8 x 18.7, -2.4°	3.7	-0.5	0.71	1.63	1.78
ECM-A11	29-OCT-12 12:57	9.028	1.59	0.14	-2.16	4.4	-3.1	22.6 x 3.6, 6.5°	-0.5	0.3	0.48	2.14	2.20
ECM-B11	29-OCT-12 12:58	9.113	5.54	0.19	-5.47	0.1	0.3	32.1 x 5.5, 4.5°	-0.1	0.3	1.68	0.13	1.68
ECM-A12	05-NOV-12 16:06	12.096	0.38	0.07	-3.07	-4.0	1.2	167.9 x 7.8, -5.4°	0.3	-0.2	0.11	1.68	1.68
ECM-B12	05-NOV-12 16:07	12.173	-4.20	0.10	-0.67	0.9	-2.5	210.6 x 12.9, -2.9°	-1.5	0.8	1.20	1.06	1.60
ECM-A13	12-NOV-12 16:14	10.954	-1.31	0.15	-1.16	-1.3	-1.3	28.4 x 3.9, 6.0°	-0.4	0.3	0.38	0.75	0.84
ECM-B13	12-NOV-12 16:15	11.116	1.93	0.32	-1.63	0.4	-5.3	43.6 x 7.7, 2.1°	-0.1	0.3	0.56	2.12	2.19
ECM-A14	19-NOV-12 19:39	5.815	1.90	0.07	-1.36	-0.1	-3.2	96.8 x 16.3, -3.6°	-0.2	0.4	0.61	1.27	1.41
ECM-B14	19-NOV-12 19:39	5.675	1.23	0.20	-2.69	-5.8	-0.5	121.8 x 20.5, 5.4°	-0.0	0.3	0.39	2.34	2.37
ECM-A15	06-DEC-12 15:34	6.805	-5.19	0.22	-0.92	-0.9	-0.2	37.1 x 10.5, 0.9°	-0.5	0.1	1.64	0.36	1.68
ECM-B15	06-DEC-12 15:35	6.862	0.20	0.19	-1.63	-7.4	-0.1	38.9 x 9.9, 5.5°	0.7	0.1	0.06	2.96	2.96
ECM-A16	10-DEC-12 17:42	11.377	-1.93	0.90	-3.71	-1.5	0.3	98.7 x 30.2, 4.5°	0.5	0.6	0.56	0.61	0.83
ECM-B16	10-DEC-12 17:42	11.376	-10.79	0.96	3.72	-0.8	-1.9	91.5 x 49.6, 5.2°	-0.2	0.5	3.13	0.80	3.23
ECM-A17	14-DEC-12 15:07	4.576	-4.79	0.49	2.19	4.8	-1.9	390.9 x 79.5, -0.5°	0.9	0.3	1.56	2.06	2.58
ECM-B17	14-DEC-12 15:07	4.519	-1.12	6.89	0.87	-0.2	-0.4	2497.5 x 2299.7, -6.4°	-2.7	1.5	0.36	0.16	0.40

Table 6. Estimate for All Main-Engine Maneuvers ($1\text{-}\sigma$)

	Fixed	Proportional
mag. bias	-2.8503 mm/s	0.0036 %
mag. std. dev.	3.0538 mm/s	0.0124 %
ptg. bias Y	-7.1773 mm/s	0.8222 mrad
ptg. bias Z	-10.2638 mm/s	0.8274 mrad
ptg. std. dev.	9.0126 mm/s	1.4643 mrad

when the excluded maneuvers are also excluded from the fitness test, see Figure 18. The result for the same model is 0.63 when the excluded maneuvers are included in the fitness test, see Figure 16.

The Q-Q plot in Fig. 17 may indicate that there are two families of data. There are 23 samples that stray from the model and seem to follow a line in that plot. On the other hand, Figs. 18 and 19 clearly show that only these seven (7) maneuvers need to be excluded to make the result acceptable. Unfortunately, the GRAIL data set may not be large enough to resolve this question.

The estimated magnitude biases in the final model, Table 6, are -2.9 mm/s fixed and 0.004% proportional which are quite different than the result for the prime mission, Table 3, which had -1.5 mm/s fixed and -0.005% proportional. For a small data set like this one, the variation in bias and the small size of the estimates seems to indicate that whatever the bias, it is too small to detect. These biases for magnitude errors were computed in the maximum-likelihood process as opposed to a weighted mean.

Table 7. “January 2013 Main Engine” (Final) Execution-Error Model ($3\text{-}\sigma$)

	Fixed	Proportional
Magnitude	9.0 mm/s	0.045 %
Pointing	0.0 mm/s	6.0 mrad

The estimated pointing biases in Table 6 were also computed in the maximum-likelihood process. These biases are larger than expected with fixed pointing biases of about 10 mm/s and 0.8 mrad proportional for each axis. Without a thorough study of possible contributors, it is difficult to assess whether these estimates may be valid. The result does indicate a smaller proportional pointing standard deviation, about 1.5 mrad instead of 2.5 mrad. Given this indication and the overall uncertainty about the pointing model, the Navigation team recommended the “January 2013 Main Engine” model in Table 7 to represent the overall execution-error performance of either GRAIL spacecraft.

CONCLUDING REMARKS

The GRAIL navigation team successfully applied maximum-likelihood estimation to determine parameters for an execution-error model common to both spacecraft. The data set was limited, totaling fifty-seven (57) maneuvers, seven (7) of which were not used to estimate the model, but were used in validation. A few issues surround the analysis that seem to mostly stem from the

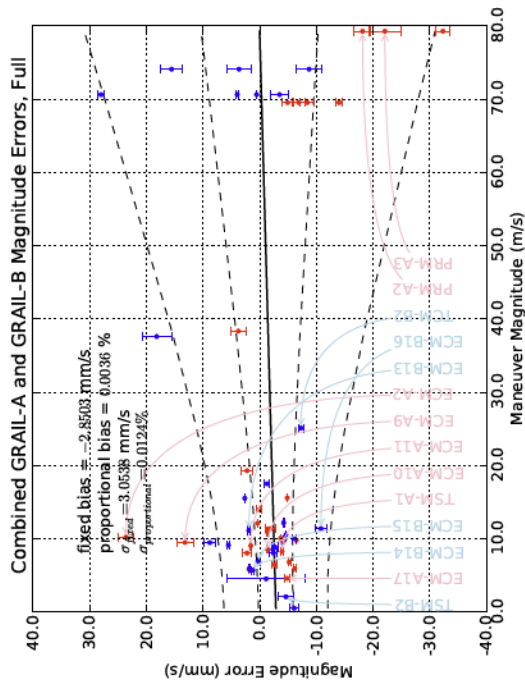


Figure 12. Final Model Mag. Residuals

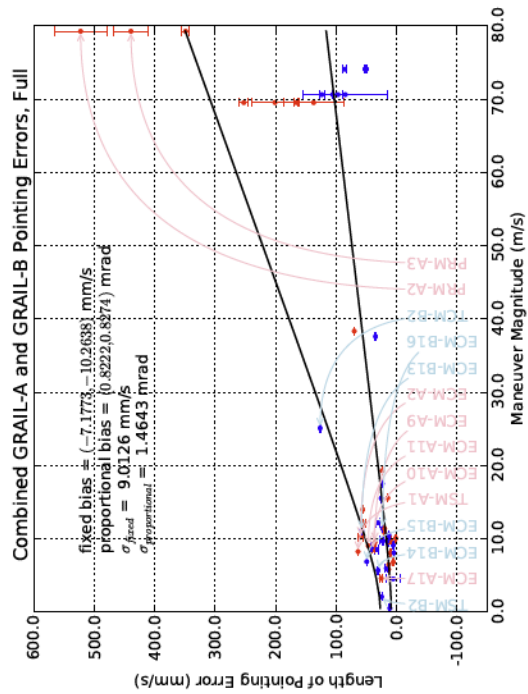


Figure 15. Final Model Ptg. Residuals

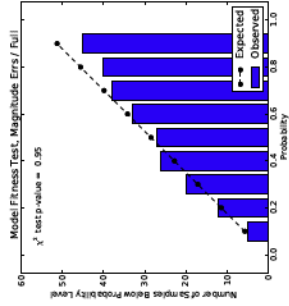


Figure 13. Final, Mag. Prob.

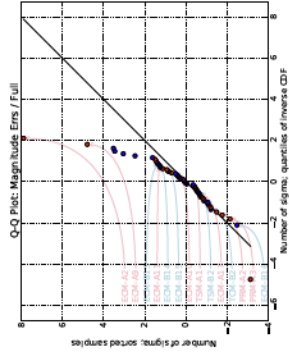


Figure 14. Final, Mag. Q-Q

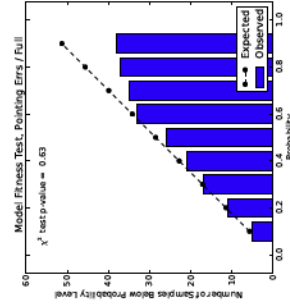


Figure 16. Final, Ptg. Prob.

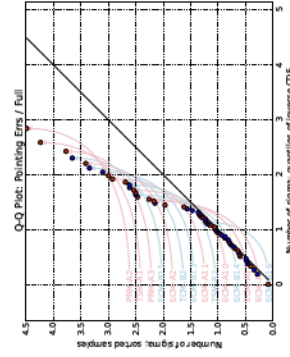


Figure 17. Final, Ptg. Q-Q

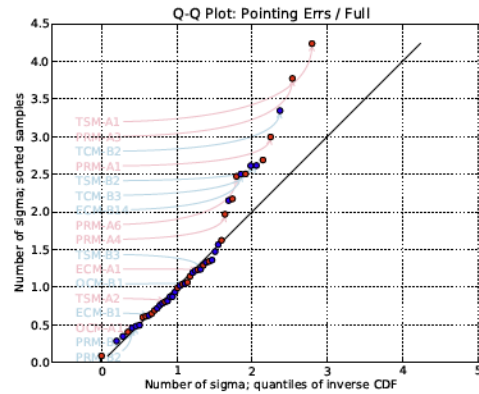
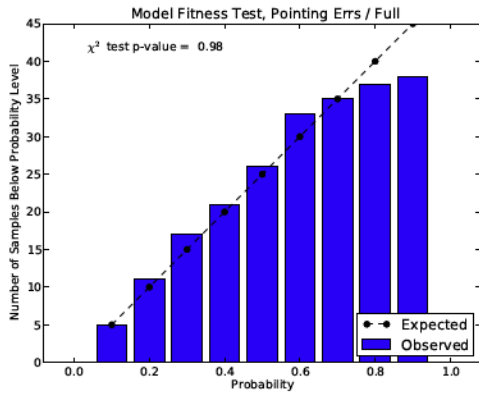


Figure 18. Final, Ptg. Prob. with Exclusions

Figure 19. Final, Ptg. Q-Q, with Exclusions

Excluded: ECM-A2, A10, A11, A17, B13, B15, and PRM-A2. Compare to Figures 16 and 17.

limited size of the data set. Without more data, it is difficult to know if the method is incorrectly reporting biases or if they are simply too small to reliably estimate. The maneuvers that were excluded from the estimation were clearly inconsistent with the rest of the data. A larger group of maneuvers may have different statistics to their pointing errors. At the same time, many members of that group seem compatible with the estimated model, according to the χ^2 test.

The data set may be too small to settle certain statistical questions as such, but is actually a relatively large number of maneuvers compared to other missions. Even if the model lacks precision, it does not lack utility. This approach produced a model that was useful for planning and flying the extended mission. Its validity was confirmed by the remaining maneuvers. These statistical methods enhance the planning and monitoring of flight projects, ultimately to help save money and fuel.

ACKNOWLEDGMENTS

This research was carried out at the Jet Propulsion Laboratory, California Institute of Technology, under a contract with the National Aeronautics and Space Administration.

REFERENCES

- [1] T. H. Sweetser, M. S. Wallace, S. J. Hatch, and R. B. Roncoli, "Design Of An Extended Mission for GRAIL," *2012 AIAA/AAS Astrodynamics Specialists Conference*, Minneapolis, Minnesota, August 2012.
- [2] C. R. Gates, "A Simplified Model of Midcourse Maneuver Execution Errors," Tech. Rep. 32-504, JPL, Pasadena, CA, October 1963.
- [3] A. Papoulis, *Probability, Random Variables, and Stochastic Processes*. New York, NY, USA: McGraw-Hill, 3rd ed., 1991.
- [4] W. E. Bollman and C. Chadwick, "Statistics of Δv Magnitude for a Trajectory Correction Maneuver Containing Deterministic and Random Components," *Proceedings of the AIAA/AAS Astrodynamics Conference, AIAA-82-1429*, San Diego, California, August 1982.
- [5] R. Roncoli and K. Fujii, *Mission Design Overview for the Gravity Recovery and Interior Laboratory (GRAIL) Mission*. American Institute of Aeronautics and Astronautics, 2010, doi:10.2514/6.2010-8383.
- [6] P. Antreasian, R. S. Bhat, S. Broschart, M.-K. Chung, K. E. Criddle, T. D. Goodson, S. J. Hatch, D. Jefferson, E. Lau, S. Mohan, J. S. Parker, R. B. Roncoli, M. Ryne, T. H. Sweetser, T.-H. You, and B. T. Young, "Navigation Of The Twin GRAIL Spacecraft Into Science Formation At The Moon," *23rd International Symposium on Space Flight Dynamics*, Pasadena, CA, 2012.

- [7] J. G. Beerer and G. Havens, "Operating the Dual-Orbiter GRAIL Mission to Measure the Moon's Gravity," *SpaceOps*, 2012.
- [8] "Gravity Recovery and Interior Laboratory (GRAIL) Project Navigation Plan, CDR Release," JPL D-44333, January 2010.
- [9] H. Lass and P. Gottlieb, *Probability and Statistics*. Addison-Wesley, 1971.
- [10] S. V. Wagner and T. D. Goodson, "Execution-Error Modeling and Analysis of the Cassini-Huygens Spacecraft Through 2007," *AAS/AIAA Space Flight Mechanics Meeting, Galveston, TX*, No. AAS 08-113, January 2008.